025921-11-T

THE UNIVERSITY OF MICHIGAN

COLLEGE OF ENGINEERING

DEPARTMENT OF ELECTRICAL ENGINEERING & COMPUTER SCIENCE

Radiation Laboratory

A NEW TECHNIQUE FOR SIMULATING COMPOSITE MATERIAL
Task 1: A Finite Element Conjugate Gradient FFT method for Scattering

Report Title: A Combined Finite Element-Boundary Element Formulation for Solution of Two-Dimensional Problems via CGFFT

Authors: Jeffery Collins, Jian-Ming Jin and John L. Volakis

Period: September 1989 - February 1990

Radiation Laboratory
Department of Electrical Engineering
and Computer Science
The University of Michigan
Ann Arbor, MI 48109-2122

National Aeronautics and
Space Administration
Ames Research Center
Moffett Field, CA 94035
Grant NAG-2-541

Ann Arbor, Michigan

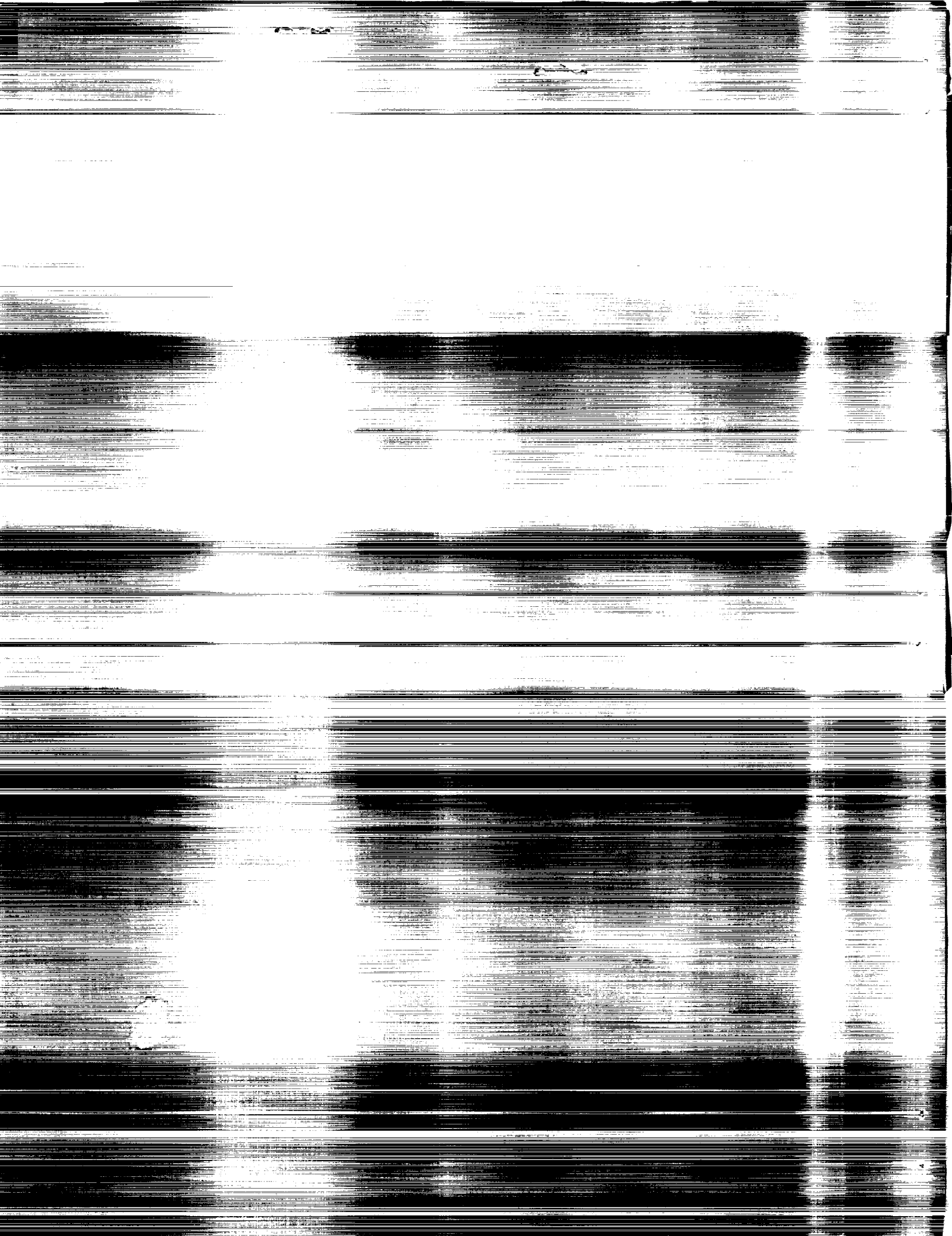

TECHNICAL REPORT

FOR

NASA Grant NAG-2-541

NASA Technical Monitor: Alex Woo

Grant Title: A NEW TECHNIQUE FOR SIMULATING COMPOSITE MATERIAL
Task 1: A Finite Element Conjugate Gradient FFT Method for Scattering

Institution: The Radiation Laboratory
Department of Electrical Engineering and Computer Science
The University of Michigan
Ann Arbor, MI 48109-2122

Period Covered: September 1989 - February 1990

Report Title: A Combined Finite Element-Boundary Element Formulation for Solution of Two-Dimensional Problems via CGFFT

Report Authors: Jeffery D. Collins, Jian-Ming Jin and John L. Volakis

Principal Investigator: John L. Volakis
Telephone: (313) 764-0500

A Combined Finite Element-Boundary Element Formulation for Solution of Two-Dimensional Problems via CGFFT

Jeffery D. Collins
Jian-Ming Jin
John L. Volakis
Radiation Laboratory
Department of Electrical Engineering and Computer Science
The University of Michigan
Ann Arbor, MI 48109-2122

Abstract

A new method for the computation of electromagnetic scattering from arbitrary two-dimensional bodies is presented. The method combines the finite element and boundary element methods leading to a system for solution via the Conjugate Gradient FFT algorithm. Two forms of boundaries aimed at reducing the storage requirement of the boundary integral are investigated. It is shown that the boundary integral becomes convolutional when a circular enclosure is chosen, resulting in reduced storage requirement when the system is solved via the Conjugate Gradient FFT method. The same holds for the ogival enclosure, except that some of the boundary integrals are not convolutional and must be carefully treated to maintain the $O(N)$ memory requirement. Results for several circular and ogival structures are presented and shown to be in excellent agreement with those obtained by traditional methods.

Contents

1 Introduction 1

2 Analysis 4

2.1 Case 1: Circular Enclosure 7

2.1.1 Discretization of the Scatterer and Field Quantities 7

2.1.2 Derivation of the Finite Element Matrix 9

2.1.3 Evaluation of the Boundary Integral 13

2.2 Case 2: Ogival Enclosure 17

2.2.1 Discretization of the Scatterer and Field Quantities 17

2.2.2 Derivation of the Finite Element Matrix 19

2.2.3 Evaluation of the Boundary Integral 20

2.3 A CGFFT Algorithm 26

3 Scattered Field Computation 29

3.1 Circular Boundary 30

3.2 Ogival Boundary 32

4 Results 35

5 Conclusions and Future Work 42

List of Figures

2.1 Geometry of the scatterer 5

2.2 Partially discretized body in a circular enclosure 7

2.3 Partially discretized body with an ogival enclosure 18

4.1 E_z and H_z bistatic echowidth from a perfectly conducting circular cylinder of radius 0.5λ. 36

4.2 E_z and H_z bistatic echowidth from a perfectly conducting circular cylinder with a conductor radius of $.5\lambda$ and a coating thickness of $.05\lambda$ containing material properties $\epsilon_r = 5 - j5$, $\mu_r = 1.5 - j0.5$. 37

4.3 E_z and H_z bistatic echowidth from a coated circular cylinder with a conductor radius of 3λ and coating thickness of 0.05λ with material properties $\epsilon_r = 5 - j5$, $\mu_r = 1.5 - j0.5$. 38

4.4 E_z and H_z backscatter echowidth from a $0.5 \times 1\lambda$ perfectly conducting ogive. 39

4.5 E_z and H_z backscatter echowidth from a $.5 \times 1\lambda$ perfectly conducting ogive with a 0.05λ thick material coating containing the properties $\epsilon_r = 3 - j5, \mu_r = 1.5 - j0.5$. 40

4.6 E_z and H_z backscatter echowidth from a $1 \times 4\lambda$ perfectly conducting ogive with a $.05\lambda$ thick material coating containing the properties $\epsilon_r = 3 - j5, \mu_r = 1.5 - j0.5$. 41

Chapter 1

Introduction

Many methods exist for the numerical solution of two-dimensional (2-D) scattering problems. Moment methods have traditionally dominated the frequency domain solution approaches though more recently, hybrid finite element methods have gained much popularity. The relative simplicity in treating complex arbitrary composite structures is a major reason for this. Also, the resulting system of equations in a finite element implementation is sparse and banded leading to a low ($O(N)$) storage required for large scale applications.

To formulate the hybrid finite element method for scattering computations, the structure is enclosed in a ficticious boundary. Within the boundary, the finite element method is used to solve a weak representation of the Helmholtz equation and further, to satisfy the radiation condition, an approximate absorbing boundary condition (ABC) [1] may be placed on the ficticious boundary. The ABC's are popular because they result in a banded sub-matrix structure. However, they require additional unknowns since the enclosure must be placed at a distance approximating the far field region. An alternative to the ABCs is to match the fields within the enclosure to an eigenfunction expansion

(unimoment method) [2] or to employ the boundary integral equation [3, 4, 6]. The unimoment method produces a dense square sub-matrix with dimension proportional to the number of modes. It also requires the truncation of an infinite series which may be slowly convergent for irregular structures thus resulting in a large storage requirement.

Previously, the authors introduced a method [6] which resulted in an $O(N)$ storage requirement. By choosing a rectangular ficticious boundary, some of the integrals in the boundary integral equation become convolutions amenable to evaluation via the fast Fourier transform (FFT). Provided the conjugate gradient (CG) algorithm is used for the solution of the system, the discretization and evaluation of the convolution integrals requires only $O(N)$ storage (while the remaining "cross-terms" must be stored in an efficient manner). Another important feature is that the order of the FFT need only be applied on the ficticious boundary making it preferable to the traditional CGFFT method, which requires the evaluation of FFTs that have the same dimensionality as that of the structure.

It is possible to choose other boundaries that result in convolutional integrals, and in this report we consider circular and ogival enclosures. Clearly, a circular enclosure would be attractive for circular scatterers whereas an ogival boundary will be more attractive for those structures conforming to this boundary. In the case of the circular boundary the entire integral is convolutional ensuring the $O(N)$ memory demand of the system provided an iterative solution is used. When an ogival enclosure is used the integral becomes convolutional only if the observation and source points are on the same arc, but an efficient storage scheme is again required for the remaining "cross-terms" [1].

[1] "cross terms" refer to integrals for which the source and observation points are not on the same arc

The hybrid finite element methods presented herein will be referred to as the combined finite element-boundary element methods (BE/FE-CGFFT), because the source and observation points associated with the boundary integral share a common contour as is the case with the traditional boundary element method [8]. In contrast, for the combined finite element - boundary integral formulation (FE-CGFFT) discussed in [6] the source and observation points are on adjacent contours. This choice of a single or double contour is, of course, arbitrary and only for convenience since in either case, the same number of unknowns are required for either case.

In the following sections, the pertinent BE/FE-CGFFT formulations are developed for the circular and ogival boundaries. Results for several circular and ogival structures are presented and shown to be in excellent agreement with that obtained by traditional methods.

Chapter 2

Analysis

Consider the plane wave [1]

$$\overline{\phi}^{inc}(\overline{\rho}) = \hat{z}\phi_z^{inc}(\overline{\rho}) = \hat{z}e^{jk_o\rho\cos(\theta-\theta_o)} \tag{2.1}$$

illuminating a composite cylinder as shown in Fig. 2.1 and we are interested in computing the scattered field. For the application of the Finite Element - Boundary Element Method the target is enclosed in a ficticious circular or ogival boundary as shown in Figs. 2.2 and 2.3. Within the boundary Γ_a, the finite element method is used to solve the Helmholtz equation

$$\nabla \cdot [v(\overline{\rho})\nabla\phi(\overline{\rho})] + k_o^2 v(\overline{\rho})\phi(\overline{\rho}) = 0 \tag{2.2}$$

where

$$\phi(\overline{\rho}) = E_z(\overline{\rho}), \quad u(\overline{\rho}) = \frac{1}{\mu_r(\overline{\rho})} \quad v(\overline{\rho}) = \epsilon_r(\overline{\rho}) \tag{2.3}$$

for E-polarization and

$$\phi(\overline{\rho}) = H_z(\overline{\rho}), \quad u(\overline{\rho}) = \frac{1}{\epsilon_r(\overline{\rho})}, \quad v(\overline{\rho}) = \mu_r(\overline{\rho}) \tag{2.4}$$

[1] An $e^{j\omega t}$ time convention is assumed and suppressed.

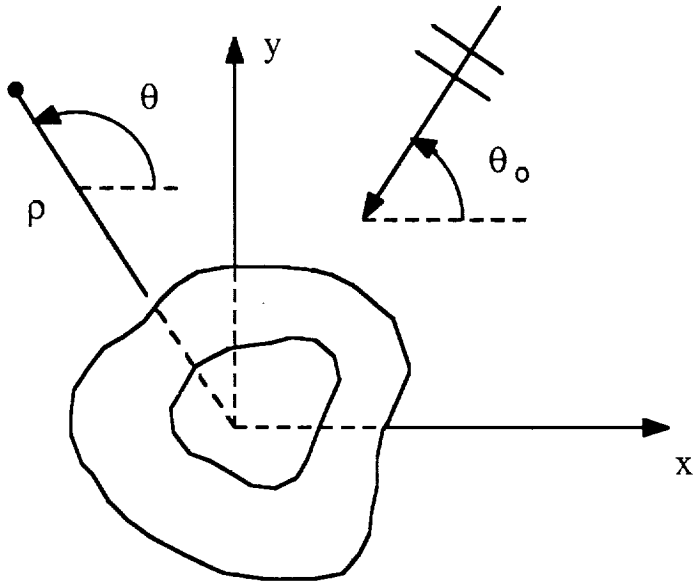

Figure 2.1: Geometry of the scatterer

for H-polarization. The free-space wave number is $k_o = \omega\sqrt{\mu_o \epsilon_o}$ and μ_r and ϵ_r are the relative permeablility and permittivity, respectively. On the boundary Γ_a the Helmholtz integral equation

$$\phi(\overline{\rho}) = \phi^{inc}(\overline{\rho}) - \oint_{\Gamma_a} \left\{ G(\overline{\rho}, \overline{\rho}_a) \left[\frac{\partial}{\partial n_a} \phi(\overline{\rho}_a) \right] - \phi(\overline{\rho}_a) \left[\frac{\partial}{\partial n_a} G(\overline{\rho}, \overline{\rho}_a) \right] \right\} dl_a \qquad (2.5)$$

provides the required boundary constraint, implicitly satisfing the radiation condition. In (2.5)

$$G(\overline{\rho}, \overline{\rho}_a) = -\frac{j}{4} H_o^{(2)}(k_o |\overline{\rho} - \overline{\rho}_a|) \qquad (2.6)$$

is the 2-D free space Green's function where $H_o^{(2)}(\cdot)$ denotes the zeroth order Hankel function of the second kind. Also, $\frac{\partial}{\partial n_a}$ denotes differentiation with respect to the outward normal, whereas $\overline{\rho}$ and $\overline{\rho}_a$ are the usual source and observation points, respectively, and

$$|\overline{\rho} - \overline{\rho}_a| = \sqrt{(x - x_a)^2 + (y - y_a)^2} \qquad (2.7)$$

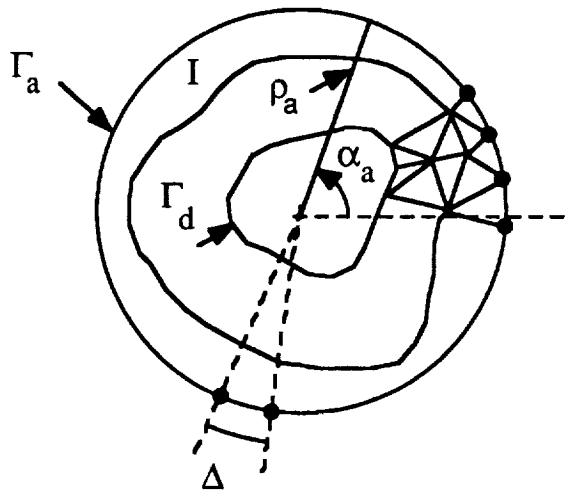

Figure 2.2: Partially discretized body in a circular enclosure

2.1 Case 1: Circular Enclosure

2.1.1 Discretization of the Scatterer and Field Quantities

The region enclosed by Γ_a, denoted as R_a, is discretized into N_e finite elements as illustrated in Fig. 2.2. In the figure, ρ_a is the radius of the circle and α_a is the integration angle along this boundary (Further definitions for the finite element mesh are indicated in Table 2.1, while the definitions of the field vectors are indicated in Table 2.2.). We note that nodes along Γ_a are equispaced with angular displacement Δ.

2.1.2 Derivation of the Finite Element Matrix

The weighted residual expression over each element may be written [9]

$$\iint_{\Omega^e} R_{\Omega^e} N_i^e d\Omega^e = 0 \quad i = 1, 2, 3 \tag{2.8}$$

Definitions for Finite Element Mesh
N_n = total number of nodes in the finite element mesh
N_g = total number of unknowns
N_e = total number of elements in the finite element mesh
N_a = number of nodes or elements on Γ_a
N_d = number of nodes or elements on Γ_d

Table 2.1: Definitions for the finite element mesh

Definitions of Field Vectors (in terms of field unknowns at nodal points)
ϕ_a = fields at the nodes on Γ_a
ψ_a = normal field derivatives at the nodes on Γ_a
ϕ_I = fields corresponding to region I enclosed by Γ_a and Γ_d
ϕ_d = fields at the nodes on Γ_d, the conductor boundary

Table 2.2: Definitions of the field vectors

where

$$R_{\Omega^e} = -\frac{\partial}{\partial x}\left[u(x,y)\frac{\partial}{\partial x}\hat{\phi}^e(x,y)\right] - \frac{\partial}{\partial y}\left[u(x,y)\frac{\partial}{\partial y}\hat{\phi}^e(x,y)\right] - k_o^2 v(x,y)\hat{\phi}^e(x,y) \quad (2.9)$$

and

$$\phi \simeq \hat{\phi} = \sum_{e=1}^{N_e} \hat{\phi}^e \quad (2.10)$$

where $\hat{\phi}^e$ is zero outside element e. In (2.9) $\hat{\phi}^e$ is an approximation to ϕ in the eth element, and N_i^e is the ith shape function associated with the eth element. Substituting (2.9) into (2.8) and invoking the divergence theorem yields

$$\iint_{\Omega^e} \left\{ -u\left[\frac{\partial\hat{\phi}^e}{\partial x}\frac{\partial N_i^e}{\partial x} + \frac{\partial\hat{\phi}^e}{\partial y}\frac{\partial N_i^e}{\partial y}\right] + k_0^2 v\hat{\phi}^e N_i^e \right\} d\Omega^e + \int_{\Gamma^e} N_i^e \hat{\psi}^e d\Gamma^e = 0 \quad (2.11)$$

where Γ^e denotes the contour enclosing the eth element. Additionally,

$$\hat{\psi}^e = u^e \frac{\partial\hat{\phi}^e}{\partial n} \quad (2.12)$$

is zero outside element e. Summing over N_e elements we obtain

$$\sum_{e=1}^{N_e} \iint_{\Omega^e} \left\{ -u\left[\frac{\partial\hat{\phi}^e}{\partial x}\frac{\partial N_i^e}{\partial x} + \frac{\partial\hat{\phi}^e}{\partial y}\frac{\partial N_i^e}{\partial y}\right] + k_0^2 v\hat{\phi}^e N_i^e \right\} d\Omega^e + \sum_{s=1}^{N_a} \int_{\Gamma_a^s} N_i^s \hat{\psi}^s d\Gamma_a^s + \sum_{s=1}^{N_d} \int_{\Gamma_d^s} N_i^s \hat{\psi}^s d\Gamma_d^s = 0 \quad (2.13)$$

where the summations over s refer to the elements with sides adjacent to the ficticious (Γ_a) and conducting (Γ_d) boundaries. The integral over the conducting boundary vanishes and if no conductor is present, then Γ_d is not present. When $\phi = H_z$, the normal derivative of the field is zero on the conductor and the field unknowns on the boundary

are allowed to "float" (i.e., the boundary condition is "naturally" satisfied). Finally, when $\phi = E_z$, imposing the Dirichlet condition during assembly of the finite element system results in the elimination of those equations associated with the integral over Γ_d.

Proceeding with the discretization, the field and its derivative within each element may be expanded into a linear combination of shape functions

$$\hat{\phi}^e = \sum_{j=1}^{3} N_j^e \hat{\phi}_j^e \tag{2.14}$$

$$\hat{\psi}^s = \sum_{k=1}^{3} N_k^s \hat{\psi}_k^s \tag{2.15}$$

Substituting (2.14) and (2.15) into (2.11) we obtain

$$\sum_{j=1}^{3} a_{ij}^e \hat{\phi}_j^e - \sum_{k=1}^{3} b_{ik}^s \hat{\psi}_k^s = 0 \tag{2.16}$$

where

$$a_{ij}^e = \iint_{\Omega^e} \left\{ u \left[\frac{\partial N_i^e}{\partial x} \frac{\partial N_j^e}{\partial x} + \frac{\partial N_i^e}{\partial y} \frac{\partial N_j^e}{\partial y} \right] - k_0^2 v N_i^e N_j^e \right\} d\Omega^e \tag{2.17}$$

and

$$b_{ik}^s = \int_{\Gamma_a^s} N_k^s N_i^s d\Gamma_a^s \tag{2.18}$$

For linear triangular elements, N_i^e are given by

$$N_i^e = \frac{1}{2\Omega^e}(a_i^e + b_i^e x + c_i^e y) \tag{2.19}$$

with

$$\Omega^e = \frac{1}{2} \det \begin{vmatrix} 1 & x_1^e & y_1^e \\ 1 & x_2^e & y_2^e \\ 1 & x_3^e & y_3^e \end{vmatrix} = \frac{1}{2}(b_i^e c_j^e - b_j^e c_i^e) \tag{2.20}$$

$$a_i^e = x_j^e y_k^e - x_k^e y_j^e \tag{2.21}$$

$$b_i^e = y_j^e - y_k^e \tag{2.22}$$

$$c_i^e = x_k^e - x_j^e \tag{2.23}$$

and (x_i^e, y_i^e) being the coordinates of the ith node of the eth element. From (2.19)

$$\frac{\partial N_i^e}{\partial x} = \frac{b_i^e}{2\Omega^e} \tag{2.24}$$

$$\frac{\partial N_i^e}{\partial y} = \frac{c_i^e}{2\Omega^e} \tag{2.25}$$

Using (2.24), (2.25) and the identity

$$\iint_{S^e} (N_1^e)^p (N_2^e)^q dx dy = 2\Omega^e \frac{p!q!}{(p+q+2)!} \tag{2.26}$$

a_{ij} in (2.17) reduces to

$$a_{ij}^e = \frac{u^e}{4\Omega^e}(b_i^e b_j^e + c_i^e c_j^e) - k_o^2 v^e \frac{\Omega^e}{12}(1+\delta_{ij}) \tag{2.27}$$

where

$$\delta_{ij} = \begin{cases} 1 \text{ if } i = j \\ 0 \text{ otherwise} \end{cases} \tag{2.28}$$

We note that in deriving (2.27) we have assumed that u and v (the reciprocal of the material constitutive parameters) are constant within each element and are given by u^e and v^e, respectively.

To find an algebraic expression for b_{ik}^s, we may reparametize the integral in (2.18) as

$$b_{ik}^s = \int_{\alpha_1}^{\alpha_1+\Delta} P_i^s P_k^s r_a d\alpha \tag{2.29}$$

where P_1^s and P_2^s are given by

$$P_1^s(\alpha) = 1 - \frac{\alpha - \alpha_1^s}{\alpha_2^s - \alpha_1^s} \tag{2.30}$$

$$P_2^s(\alpha) = \frac{\alpha - \alpha_1^s}{\alpha_2^s - \alpha_1^s} \tag{2.31}$$

Integrating, we have

$$b_{ik}^s = \frac{r_a \Delta}{6}(\delta_{ik} + 1) \tag{2.32}$$

Substituting the previous equations into (2.13) a sparse matrix is obtained for the nodal fields that has the form

$$\begin{bmatrix} A_{aa} & A_{aI} & 0 & -B_{aa} \\ A_{Ia} & A_{II} & A_{Id} & 0 \\ 0 & A_{dI} & A_{dd} & 0 \\ 0 & 0 & 0 & 0 \end{bmatrix} \begin{bmatrix} \phi_a \\ \phi_I \\ \phi_d \\ \psi_a \end{bmatrix} = \begin{bmatrix} 0 \\ 0 \\ 0 \\ 0 \end{bmatrix} \tag{2.33}$$

In this, the values of the elements in the submatrix A_{pq} are the contributions associated with the nodes in group (region or boundary) p which are connected directly to the nodes in group q. Also,

$$[B_{aa}]_{ik} = \sum_{s=1}^{N_a} b_{ik}^s = \frac{r_a \Delta}{6}(\delta_{i-1,k} + 4\delta_{ik} + \delta_{i+1,k}) \tag{2.34}$$

The last row in (2.33) has been intentionally left blank to imply a need for another set of equations relating the fields and its derivatives on Γ_a. This additional set of equations is produced by discretizing the boundary integral equation.

The last row in (2.33) has been intentionally left blank to imply a need for another set of equations relating the fields and its derivatives on Γ_a. This additional set of equations is produced by discretizing the boundary integral equation.

2.1.3 Evaluation of the Boundary Integral

The boundary integral in (2.5) may be rewritten in cylindrical coordinates via the transformations

$$\begin{aligned} |\overline{\rho} - \overline{\rho}_a| &= |\hat{x}(\rho\cos\alpha - \rho_a\cos\alpha_a) - \hat{y}(\rho\sin\alpha - \rho_a\sin\alpha_a)| \\ &= \sqrt{\rho^2 + \rho_a^2 - 2\rho\rho_a\cos(\alpha - \alpha_a)} \end{aligned} \tag{2.35}$$

where (ρ, α) and (ρ_a, α_a) are the usual source and observation points in cylindrical coordinates. For $|\rho| = |\rho_a|$,

$$|\overline{\rho} - \overline{\rho}_a| = 2\rho\,|\sin(\tfrac{\alpha-\alpha_a}{2})| \tag{2.36}$$

and the Green's function and its normal derivative may be written as

$$G(\overline{\rho}, \overline{\rho}_a) = -\frac{j}{4}H_o^{(2)}(2k_o\rho_a\sin(\tfrac{\alpha-\alpha_a}{2})) \tag{2.37}$$

$$\frac{\partial}{\partial n_a}G(\overline{\rho}, \overline{\rho}_a) = \frac{jk_o}{4}H_1^{(2)}(2k_o\rho_a\sin(\tfrac{\alpha-\alpha_a}{2}))\sin(\tfrac{\alpha-\alpha_a}{2}). \tag{2.38}$$

We may now write (2.5) as [8]

$$\frac{1}{2}\phi(\rho,\alpha) = \phi^{inc}(\rho,\alpha) - f_0(\rho,\alpha) + f_1(\rho,\alpha) \tag{2.39}$$

where as a result of (2.37) and (2.38)

$$f_0(\rho,\alpha) = -\frac{j}{4}\rho_a \int_0^{2\pi} \psi(\rho_a,\alpha_a)H_o^{(2)}(2k_o\rho_a\sin(\tfrac{\alpha-\alpha_a}{2}))\,d\alpha_a \tag{2.40}$$

$$f_1(\rho,\alpha) = \frac{j}{4}\rho_a \fint_0^{2\pi} \phi(\rho_a,\alpha_a) H_1^{(2)}\left(2k_o\rho_a \sin\left(\tfrac{\alpha-\alpha_a}{2}\right)\right) \sin\left(\tfrac{\alpha-\alpha_a}{2}\right) d\alpha_a \tag{2.41}$$

with

$$\psi(\rho_a,\alpha_a) = \frac{\partial}{\partial\rho_a}\phi(\rho_a,\alpha_a) \tag{2.42}$$

The factor of $\frac{1}{2}$ in (2.39) accounts for the singularity associated with $H_1^{(2)}(\cdot)$ and the $\fint$ in (2.40) and (2.41) denotes principle value.

We may now discretize (2.40) by expanding the field using pulse basis functions as

$$\psi(\rho_a,\alpha_a) \simeq \sum_{j=1}^{N_a} P_\Delta(\alpha_a - \alpha_j)\hat{\psi}_j \tag{2.43}$$

where

$$P_\Delta(\alpha_a - \alpha_j) = \begin{cases} 1 & |\alpha_a - \alpha_j| \le \frac{\Delta}{2} \\ 0 & \text{otherwise} \end{cases} \tag{2.44}$$

and Δ is the angular width of the integration cell as indicated in Fig. 2.2. Thus, the discrete version of (2.40) may be written as

$$f_0(\rho,\alpha) = -\frac{j\rho_a}{4}\sum_{j=1}^{N_a}\hat{\psi}_j \fint_{\alpha_j-\frac{\Delta}{2}}^{\alpha_j+\frac{\Delta}{2}} H_o^{(2)}\left(2k_o\rho_a \sin\left(\tfrac{\alpha-\alpha_a}{2}\right)\right) d\alpha_a \tag{2.45}$$

Performing point collocation and letting $u' = \alpha - \alpha_a$, we have

$$f_0(\rho,\alpha_i) = -\frac{j\rho_a}{4}\sum_{j=1}^{N_a}\hat{\psi}_j \fint_{(\alpha_i-\alpha_j)-\frac{\Delta}{2}}^{(\alpha_i-\alpha_j)+\frac{\Delta}{2}} H_o^{(2)}\left(2k_o\rho_a \sin\left(\tfrac{u'}{2}\right)\right) du' \tag{2.46}$$

which may be written in compact form as

$$f_0(\rho,\alpha_i) = -\frac{j\rho_a}{4}\sum_{j=1}^{N_a}\hat{\psi}_j h_0(\alpha_i - \alpha_j) \tag{2.47}$$

where

$$h_0(\alpha_i - \alpha_j) = \fint_{(\alpha_i-\alpha_j)-\frac{\Delta}{2}}^{(\alpha_i-\alpha_j)+\frac{\Delta}{2}} H_o^{(2)}\left(2k_o\rho_a \sin\left(\tfrac{u}{2}\right)\right) du \tag{2.48}$$

It is clear that (2.47) is in the form of a discrete convolution and can thus be written as

$$f_0(\rho,\alpha) = DFT^{-1}\left\{DFT(\hat{\psi}) \bullet DFT(h_0)\right\} \tag{2.49}$$

where the elements of h_0 are given by

$$h_0(p\Delta) = \begin{cases} \Delta\left\{1 - j\frac{2}{\pi}\left[\ln\left(\frac{\gamma k_0\rho_a\Delta}{4}\right) - 1\right]\right\} & p = 0 \\ \int_{(p-\frac{1}{2})\Delta}^{(p+\frac{1}{2})\Delta} H_o^{(2)}\left(2k_o\rho_a \sin\left(\frac{u'}{2}\right)\right) du' & p = 1,...,N_a - 1 \end{cases} \tag{2.50}$$

and $\gamma \simeq 1.781$ [10]. Through a similar analysis, the field may be approximated by the expansion

$$\phi(\rho_a,\alpha_a) \simeq \sum_{j=1}^{N_a} P_\Delta(\alpha_a - \alpha_j)\hat{\phi}_j \tag{2.51}$$

and by substutiting this into (2.41), we obtain

$$f_1(\rho,\alpha_i) = j\frac{k_0\rho_a}{4}\sum_{j=1}^{N_a}\phi_j h_1(\alpha_i - \alpha_j) \tag{2.52}$$

where

$$h_1(\alpha_i - \alpha_j) = \int_{(\alpha_i-\alpha_j)-\frac{\Delta}{2}}^{(\alpha_i-\alpha_j)+\frac{\Delta}{2}} H_1^{(2)}\left(2k_o\rho_a \sin\left(\tfrac{u'}{2}\right)\right)\sin\left(\tfrac{u'}{2}\right) du' \tag{2.53}$$

Clearly, (2.52) may again be written in operator form as

$$f_1(\rho,\alpha) = DFT^{-1}\left\{DFT(\hat{\phi}) \bullet DFT(h_1)\right\} \tag{2.54}$$

where

$$h_1(p\Delta) = \begin{cases} k_0\rho_a\left(\frac{\Delta}{2} - \sin\frac{\Delta}{2}\right) + j\frac{\Delta}{\pi k_0\rho_a} & p = 0 \\ \int_{(p-\frac{1}{2})\frac{\Delta}{2}}^{(p+\frac{1}{2})\frac{\Delta}{2}} H_1^{(2)}\left(2k_o\rho_a \sin\left(\frac{u'}{2}\right)\right)\sin\left(\frac{u'}{2}\right) du' & p = 1,...,N_a - 1 \end{cases} \tag{2.55}$$

Point matching (2.39) at each node results in the system

$$\frac{1}{2}\phi_i = \phi_i^{inc} - f_0(\rho,\alpha_i) + f_1(\rho,\alpha_i) \tag{2.56}$$

which may be written in operator form as

$$M_{aa}\phi_a - L_{aa}\psi_a = \phi_a^{inc} \tag{2.57}$$

where

$$[L_{aa}]_{ij} = \frac{j\rho_a}{4} h_0(\alpha_i - \alpha_j) \tag{2.58}$$

$$[M_{aa}]_{ij} = \frac{1}{2}\delta_{ij} - \frac{j\rho_a k_0}{4} h_1(\alpha_i - \alpha_j) \tag{2.59}$$

A final system is obtained by combining (2.57) with (2.33) to yield

$$\begin{bmatrix} A_{aa} & A_{aI} & 0 & -B_{aa} \\ A_{Ia} & A_{II} & A_{Id} & 0 \\ 0 & A_{dI} & A_{dd} & 0 \\ M_{aa} & 0 & 0 & -L_{aa} \end{bmatrix} \begin{bmatrix} \phi_a \\ \phi_I \\ \phi_d \\ \psi_a \end{bmatrix} = \begin{bmatrix} 0 \\ 0 \\ 0 \\ \phi_a^{inc} \end{bmatrix} \tag{2.60}$$

which can be solved via the conjugate gradient algorithm to obtain the nodal fields.

Definitions for Finite Element Mesh
N_n = total number of nodes in the finite element mesh
N_g = total number of unknowns
N_e = total number of elements in the finite element mesh
$N_a = N_{a_1} + N_{a_2}$ = number of nodes on Γ_a
$\Gamma_a = \Gamma_{a_1} + \Gamma_{a_2}$

Table 2.3: Definitions for the finite element mesh

2.2 Case 2: Ogival Enclosure

2.2.1 Discretization of the Scatterer and Field Quantities

The region within Γ_a, denoted R_a, is discretized into N_e finite elements and a partial discretization is shown in Fig. 2.3 for the circular case. In Fig. 2.3,

Δ_p = angular displacement between nodes on Γ_{a_p}
ρ_{a_p} = radii of Γ_{a_p}
α_{a_p} = angular integration variable along Γ_{a_p}
t = distance between centers of curvature of Γ_{a_p}
y_{c_p} = y-coordinate of the center of curvature of Γ_{a_p}

Further definitions for the finite element mesh are indicated in Table 2.3, and the field vector definitions are indicated in Table 2.4.

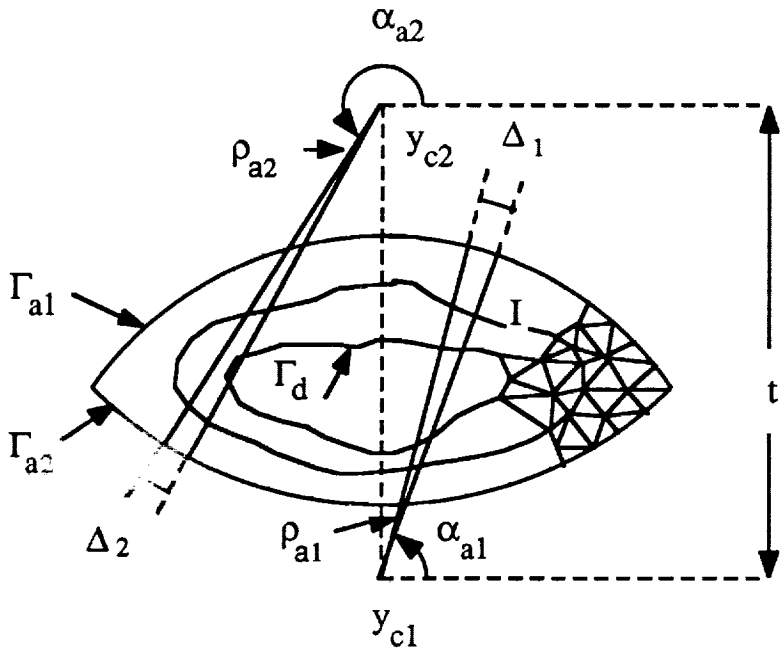

Figure 2.3: Partially discretized body with an ogival enclosure

Definitions of Field Vectors (in terms of field unknowns at nodal points)
ϕ_{a_p} = fields corresponding to the nodes on Γ_{a_p}, $p = 1, 2$
ψ_{a_p} = fields corresponding to the midpoints of the nodes on Γ_{a_p}
φ_{a_p} = fields at the nodal midpoints on Γ_{a_p}
ϕ_I = fields corresponding to region I enclosed by Γ_a and Γ_d
ϕ_d = fields corresponding to the nodes on the Γ_d

Table 2.4: Definitions of the field vectors

2.2.2 Derivation of the Finite Element Matrix

The derivation of the finite element matrix follows that described in section 2.1.1 with the exception of the matrix B_{aa}. Consider the ogival boundary as indicated in fig. 2.3. The boundary contour Γ_a is comprised of two arcs labeled Γ_{a_1} and Γ_{a_2}, which form the vertices of the ogive where they meet. At the vertices the unknown normal field is discontinuous and will therefore be evaluated at the midpoint. Also, in evaluating the contour integral, the field derivative will be expanded in terms of pulse basis functions, rather than linear functions. This results in a different B_{aa} matrix and involves the replacement of P_j^e in (2.29) by the pulse basis function expansion

$$P_\Delta(\alpha - \alpha_j) = \begin{cases} 1 & \text{if } 0 \le |\alpha - \alpha_j| \le \frac{\Delta}{2} \\ 0 & \text{otherwise} \end{cases} \tag{2.61}$$

By integrating in cylindrical coordinates we then obtain

$$b_{ij}^e = \frac{l^e}{2}(\delta_{ij} + \delta_{i,j+1}), \quad j = 1, \ i = 1,2 \tag{2.62}$$

where l^e is the length of the eth boundary element along Γ_a and is equal to $\rho_{a_p}\Delta_p$ for Γ_{a_p}, $p = 1, 2$. Performing a summation over all boundary elements then yields

$$[B_{aa}]_{ij} = \sum_{e=1}^{N_e} b_{ij}^e = \frac{l^j}{2}(\delta_{ij} + \delta_{i,j+1}) \tag{2.63}$$

where l^j is the length of the jth element since the jth "node" (associated with the unknown ψ_j) is at the center of the jth boundary element.

The remainder of finite element analysis for this case proceeds exactly as in section 2.1.2.

2.2.3 Evaluation of the Boundary Integral

The evaluation of the boundary integral along an ogival contour is similar to that described for the circular boundary. For integration and observation points on the same arc, the integrals become convolutions. On the other hand, when the integration and observation points reside on different contours, the integrals have no special form and must be discretized and stored in memory as efficiently as possible.

The distance between the source and observation points in terms of cylindrical coordinates for points on the same arc is given by

$$|\overline{\rho} - \overline{\rho}_{a_p}| = \sqrt{\rho^2 + \rho_{a_p}^2 - 2\rho\rho_{a_p}\cos(\alpha - \alpha_{a_p})} \quad p = 1,2 \tag{2.64}$$

When the source and observation points are along different arcs, (2.64) becomes

$$|\overline{\rho}_q - \overline{\rho}_{a_p}| = \sqrt{(\rho\cos\alpha_q - \rho_a\cos\alpha_{a_p})^2 + (\rho\sin\alpha_q - \rho_a\sin\alpha_{a_p} + y_{c_q} - y_{c_p})^2}$$

$$p,q = 1,2 \tag{2.65}$$

in which the subscript a_p refers to the integration coordinates along contour p and the subscript q refers to the observation coordinates. Also, y_{c_p} is the y-coordinate of the center of curvature for contour p for $p = 1,2$. For further reference we note that (2.65) may be also rewritten as

$$|\overline{\rho}_{\substack{1\\2}} - \overline{\rho}_{a_{\substack{2\\1}}}| = \sqrt{(\rho_{\substack{1\\2}}^2 + \rho_{a_{\substack{2\\1}}}^2 - 2\rho_{\substack{1\\2}}\rho_{a_{\substack{2\\1}}}\cos(\alpha_{\substack{1\\2}} - \alpha_{a_{\substack{2\\1}}}) + t^2 \mp 2t(\rho_{\substack{1\\2}}\sin\alpha_{\substack{1\\2}} - \rho_{a_{\substack{2\\1}}}\sin\alpha_{a_{\substack{2\\1}}})} \tag{2.66}$$

where $t = y_{c_2} - y_{c_1}$.

To discretize (2.5), the fields are expanded as

$$\phi(\rho_a, \alpha_a) \simeq \sum_{j=1}^{N_{a_1}} P_\Delta(\alpha_a - \alpha_j)\hat{\varphi}_j + \sum_{j=N_{a_1}+1}^{N_a} P_\Delta(\alpha_a - \alpha_j)\hat{\varphi}_j \tag{2.67}$$

$$\psi(\rho_a, \alpha_a) \simeq \sum_{j=1}^{N_{a_1}} P_\Delta(\alpha_a - \alpha_j)\hat{\psi}_j + \sum_{j=N_{a_1}+1}^{N_a} P_\Delta(\alpha_a - \alpha_j)\hat{\psi}_j \tag{2.68}$$

where as before

$$P_\Delta(\alpha_a - \alpha_j) = \begin{cases} 1 & \text{if } |\alpha_a - \alpha_j| \leq \frac{\Delta}{2} \\ 0 & \text{otherwise} \end{cases} \tag{2.69}$$

and

$$\hat{\varphi}_j = \frac{1}{2}(\hat{\phi}_j + \hat{\phi}_{j+1}) \tag{2.70}$$

Substutiting (2.67), (2.68) and (2.69) into (2.5) then yields

$$\begin{aligned} \frac{1}{2}\phi(\rho_1, \alpha_1) = \phi^{inc}(\rho_1, \alpha_1) - \Bigg\{ & \sum_{j=1}^{N_{a_1}} \hat{\psi}_j \fint_{\alpha_j}^{\alpha_j+\Delta_1} G_o(\rho_1, \rho_{a_1}, \alpha_1 - \alpha_{a_1})\rho_{a_1} d\alpha_{a_1} \\ & + \sum_{j=N_{a_1}+1}^{N_a} \hat{\psi}_j \fint_{\alpha_j}^{\alpha_j+\Delta_2} G_o(\rho_1, \rho_{a_2}, \alpha_1, \alpha_{a_2})\rho_{a_2} d\alpha_{a_2} \\ & - \sum_{j=1}^{N_{a_1}} \hat{\varphi}_j \fint_{\alpha_j}^{\alpha_j+\Delta_1} \frac{\partial}{\partial \rho_{a_1}} G_o(\rho_1, \rho_{a_1}, \alpha_1 - \alpha_{a_1})\rho_{a_1} d\alpha_{a_1} \\ & - \sum_{j=N_{a_1}+1}^{N_a} \hat{\varphi}_j \fint_{\alpha_j}^{\alpha_j+\Delta_2} \frac{\partial}{\partial \rho_{a_2}} G_o(\rho_1, \rho_{a_2}, \alpha_1, \alpha_{a_2})\rho_{a_2} d\alpha_{a_2} \Bigg\} \end{aligned} \tag{2.71}$$

when the observation point is on Γ_{a_1} and

$$\begin{aligned} \frac{1}{2}\phi(\rho_2, \alpha_2) = \phi^{inc}(\rho_2, \alpha_2) - \Bigg\{ & \sum_{j=1}^{N_{a_1}} \hat{\psi}_j \fint_{\alpha_j}^{\alpha_j+\Delta_1} G_o(\rho_2, \rho_{a_1}, \alpha_2, \alpha_{a_1})\rho_{a_1} d\alpha_{a_1} \\ & + \sum_{j=N_{a_1}+1}^{N_a} \hat{\psi}_j \fint_{\alpha_j}^{\alpha_j+\Delta_2} G_o(\rho_2, \rho_{a_2}, \alpha_2 - \alpha_{a_2})\rho_{a_2} d\alpha_{a_2} \end{aligned}$$

$$- \sum_{j=1}^{N_{a_1}} \hat{\varphi}_j \int_{\alpha_j}^{\alpha_j+\Delta_1} \frac{\partial}{\partial \rho_{a_1}} G_o(\rho_2, \rho_{a_1}, \alpha_2, \alpha_{a_1}) \rho_{a_1} d\alpha_{a_1}$$

$$- \sum_{j=N_{a_1}+1}^{N_a} \hat{\varphi}_j \int_{\alpha_j}^{\alpha_j+\Delta_2} \frac{\partial}{\partial \rho_{a_2}} G_o(\rho_2, \rho_{a_2}, \alpha_2 - \alpha_{a_2}) \rho_{a_2} d\alpha_{a_2} \Big\} \qquad (2.72)$$

for observation on Γ_{a_2}. Performing point collocation at the nodal midpoints, (2.71) and (2.72) further reduce to

$$\frac{1}{2}\phi(\rho_1, \alpha_{i+\frac{1}{2}}) = \phi^{inc}(\rho_1, \alpha_{i+\frac{1}{2}}) - \Big\{ \sum_{j=1}^{N_{a_1}} \hat{\psi}_j \int_{\alpha_i-\alpha_j+\frac{\Delta}{2}}^{\alpha_i-\alpha_j+\frac{\Delta}{2}} G_o(\rho_1, \rho_{a_1}, u) \rho_{a_1} du$$

$$+ \sum_{j=N_{a_1}+1}^{N_a} \hat{\psi}_j \int_{\alpha_j}^{\alpha_j+\Delta_2} G_o(\rho_1, \rho_{a_2}, \alpha_{i+\frac{1}{2}}, \alpha_{a_2}) \rho_{a_2} d\alpha_{a_2}$$

$$- \sum_{j=1}^{N_{a_1}} \hat{\varphi}_j \int_{\alpha_i-\alpha_j+\frac{\Delta}{2}}^{\alpha_i-\alpha_j+\frac{\Delta}{2}} \frac{\partial}{\partial \rho_{a_1}} G_o(\rho_1, \rho_{a_1}, u) \rho_{a_1} du$$

$$- \sum_{j=N_{a_1}+1}^{N_a} \hat{\varphi}_j \int_{\alpha_j}^{\alpha_j+\Delta_2} \frac{\partial}{\partial \rho_{a_2}} G_o(\rho_1, \rho_{a_2}, \alpha_{i+\frac{1}{2}}, \alpha_{a_2}) \rho_{a_2} d\alpha_{a_2} \Big\} \qquad (2.73)$$

for observation on Γ_{a_1} and

$$\frac{1}{2}\phi(\rho_2, \alpha_{i+\frac{1}{2}}) = \phi^{inc}(\rho_2, \alpha_{i+\frac{1}{2}}) - \Big\{ \sum_{j=1}^{N_{a_1}} \hat{\psi}_j \int_{\alpha_j}^{\alpha_j+\Delta_1} G_o(\rho_2, \rho_{a_1}, \alpha_{i+\frac{1}{2}}, \alpha_{a_1}) \rho_{a_1} d\alpha_{a_1}$$

$$+ \sum_{j=N_{a_1}+1}^{N_a} \hat{\psi}_j \int_{\alpha_i-\alpha_j+\frac{\Delta}{2}}^{\alpha_i-\alpha_j+\frac{\Delta}{2}} G_o(\rho_2, \rho_{a_2}, u) \rho_{a_2} du$$

$$- \sum_{j=1}^{N_{a_1}} \hat{\varphi}_j \int_{\alpha_j}^{\alpha_j+\Delta_1} \frac{\partial}{\partial \rho_{a_1}} G_o(\rho_2, \rho_{a_1}, \alpha_{i+\frac{1}{2}}, \alpha_{a_1}) \rho_{a_1} d\alpha_{a_1}$$

$$- \sum_{j=N_{a_1}+1}^{N_a} \hat{\varphi}_j \int_{\alpha_i-\alpha_j+\frac{\Delta}{2}}^{\alpha_i-\alpha_j+\frac{\Delta}{2}} \frac{\partial}{\partial \rho_{a_2}} G_o(\rho_2, \rho_{a_2}, u) \rho_{a_2} du \Big\} \qquad (2.74)$$

where the '$\frac{1}{2}$' in the subscript refers to the ficticious "node" midway between the actual nodes. A system of equations can now be obtained by testing (2.73) and (2.74) at a sequence of points on the contours. This yields

$$\frac{1}{4} C_1 \phi_{a_1} = \varphi_{a_1}^{inc} - \Big\{ L_{11}\psi_{a_1} + P_{12}\psi_{a_2} - \frac{1}{2} M_{11} C_1 \phi_{a_1} - \frac{1}{2} Q_{12} C_2 \phi_{a_2} \Big\}$$

$$\frac{1}{4}C_2\phi_{a_2} = \varphi_{a_2}^{inc} - \left\{ P_{21}\psi_{a_1} + L_{22}\psi_{a_2} - \frac{1}{2}Q_{21}C_1\phi_{a_1} - \frac{1}{2}M_{22}C_2\phi_{a_2} \right\} \tag{2.75}$$

which can be alternatively written as

$$\left[\begin{bmatrix} \mathcal{M}_{11}C_1 & \mathcal{Q}_{12}C_2 \\ \mathcal{Q}_{21}C_1 & \mathcal{M}_{22}C_2 \end{bmatrix} \begin{bmatrix} D \end{bmatrix} \begin{bmatrix} L_{11} & P_{12} \\ P_{21} & L_{22} \end{bmatrix} \right] \begin{bmatrix} \phi_{a_1} \\ \phi_{a_2} \\ \psi_{a_1} \\ \psi_{a_2} \end{bmatrix} = \begin{bmatrix} \varphi_{a_1}^{inc} \\ \varphi_{a_2}^{inc} \end{bmatrix} \tag{2.76}$$

In this C is a matrix with 1's down the main and super diagonals, and $\varphi_{a_p}^{inc}$ are the value of the incident field evaluated at the nodal midpoints. The matrix D accounts for the double use of the nodes at the endpoints and the remaining elements are given by

$$\mathcal{M}_{pp} = \frac{1}{2}(\frac{1}{2}I - M_{pp}) \tag{2.77}$$

$$\mathcal{Q}_{pq} = -\frac{1}{2}Q_{pq} \tag{2.78}$$

$$\tag{2.79}$$

for $p = 1, 2$ in which

$$[M_{pp}]_{ij} = \int_{\alpha_i - \alpha_j + \frac{\Delta_p}{2}}^{\alpha_i - \alpha_j + \frac{\Delta_p}{2}} G_o(\rho_p, \rho_{a_p}, u)\rho_{a_p} du \tag{2.80}$$

$$[L_{pp}]_{ij} = \int_{\alpha_i - \alpha_j + \frac{\Delta_p}{2}}^{\alpha_i - \alpha_j + \frac{\Delta_p}{2}} \frac{\partial}{\partial \rho_{a_p}} G_o(\rho_p, \rho_{a_p}, u)\rho_{a_p} du \tag{2.81}$$

$$[Q_{pq}]_{ij} = \int_{\alpha_j}^{\alpha_j + \Delta_q} G_o(\rho_p, \rho_{a_q}, \alpha_{i+\frac{1}{2}}, \alpha_{a_q})\rho_{a_q} d\alpha_{a_q} \tag{2.82}$$

and

$$[P_{pq}]_{ij} = \int_{\alpha_j}^{\alpha_j + \Delta_q} \frac{\partial}{\partial \rho_{a_q}} G_o(\rho_p, \rho_{a_q}, \alpha_{i+\frac{1}{2}}, \alpha_{a_q})\rho_{a_q} d\alpha_{a_q} \tag{2.83}$$

More explicitly, upon evaluation of the integrals

$$[M_{pp}]_{ij} = \begin{cases} j\frac{k_o\rho_{a_p}}{4}\left[k_o\rho_{a_p}(\frac{\Delta_p}{2} - \sin\frac{\Delta_p}{2}) + \frac{j\Delta_p}{\pi k_o\rho_{a_p}}\right] & i = j \\ j\frac{k_o\rho_{a_p}}{4}\int_{\alpha_i-\alpha_j+\frac{\Delta_p}{2}}^{\alpha_i-\alpha_j+\frac{\Delta_p}{2}} H_1^{(2)}(2k_o\rho_{a_p}\sin\frac{u}{2})\sin\frac{u}{2}du & i \neq j \end{cases} \tag{2.84}$$

$$[L_{pp}]_{ij} = \begin{cases} -j\frac{k_o\rho_{a_p}}{4}\left\{1 - j\frac{2}{\pi}\left[\ln\left(\frac{\gamma k_o\rho_{a_p}\Delta_p}{4}\right) - 1\right]\right\} & i = j \\ -j\frac{\rho_{a_p}}{4}\int_{\alpha_i-\alpha_j+\frac{\Delta_p}{2}}^{\alpha_i-\alpha_j+\frac{\Delta_p}{2}} H_o^{(2)}(2k_o\rho_{a_p}\sin\frac{u}{2})du & i \neq j \end{cases} \tag{2.85}$$

$$\left[Q_{\substack{12\\21}}\right]_{ij} = j\frac{k_o\rho_{a_{\substack{2\\1}}}}{4}\int_{\alpha_j}^{\alpha_j+\Delta_{\substack{2\\1}}} \frac{H_1^{(2)}(k_o\sqrt{\cdot \mp t\cdot})}{(k_o\sqrt{\cdot \mp t\cdot})} \left[\rho_{a_{\substack{2\\1}}} - \rho_{\substack{1\\2}}\cos(\alpha_{\substack{1\\2}} - \alpha_{a_{\substack{2\\1}}}) \pm t\sin\alpha_{a_{\substack{2\\1}}}\right] d\alpha_{a_{\substack{2\\1}}} \tag{2.86}$$

$$\left[P_{\substack{12\\21}}\right]_{ij} = -j\frac{\rho_{a_{\substack{2\\1}}}}{4}\int_{\alpha_j}^{\alpha_j+\Delta_{\substack{2\\1}}} H_o^{(2)}(k_o\sqrt{\cdot \mp t\cdot})d\alpha_{a_{\substack{2\\1}}} \tag{2.87}$$

where the upper sign corresponds to the upper set of subscripts on P or Q, while the lower sign corresponts to the lower set of subscripts. Introducing the definitions

$$K_1 = \begin{bmatrix} \mathcal{M}_{11}C_1 & \mathcal{Q}_{12}C_2 \\ \mathcal{Q}_{21}C_1 & \mathcal{M}_{22}C_2 \end{bmatrix}\begin{bmatrix} D \end{bmatrix} \tag{2.88}$$

$$K_2 = \begin{bmatrix} L_{11} & P_{12} \\ P_{21} & L_{22} \end{bmatrix} \tag{2.89}$$

the system (2.76) may be combined with that derived via the finite element method to obtain

$$\begin{bmatrix} A_{aa} & A_{aI} & 0 & -B_{aa} \\ A_{Ia} & A_{II} & A_{Id} & 0 \\ 0 & A_{dI} & A_{dd} & 0 \\ K_1 & 0 & 0 & K_2 \end{bmatrix}\begin{bmatrix} \phi_a \\ \phi_I \\ \phi_d \\ \psi_a \end{bmatrix} = \begin{bmatrix} 0 \\ 0 \\ 0 \\ \varphi_a^{inc} \end{bmatrix} \tag{2.90}$$

We note that (2.90) can be solved via the CG algorithm to take advantage of the convolution operators M and L in reducing the memory requirements. This algorithm is given next.

2.3 A CGFFT Algorithm

The CG algorithm to be employed for solving a system of the form

$$A\phi = b \tag{2.91}$$

as in (2.60) and (2.90) is as follows:

Initialize the residual and search vectors

$$\gamma_b = \| [\ \phi^{inc} \quad 0 \quad 0 \quad 0\ ]^T \|_2^2 = \| b \|_2^2 \tag{2.92}$$

$$s = A\phi^{(0)} \tag{2.93}$$

$$r^{(1)} = b - s$$

$$s = A^a r^{(1)} \tag{2.94}$$

$$\gamma_s = \| s \|_2^2 \tag{2.95}$$

$$\beta^{(0)} = \gamma_s^{-1} \tag{2.96}$$

$$p^{(1)} = \beta^{(0)} s \tag{2.97}$$

Iterate for $k = 1, ..., N_g$

$$s = Ap^{(k)} \tag{2.98}$$

$$\gamma_s = \| s \|_2^2 \tag{2.99}$$

$$\alpha^{(k)} = \gamma_s^{-1} \tag{2.100}$$

$$\phi^{(k+1)} = \phi^{(k)} + \alpha^{(k)} p^{(k)} \tag{2.101}$$

$$r^{(k+1)} = r^{(k)} - \alpha^{(k)} p^{(k)} \tag{2.102}$$

$$\gamma_r = \| r^{(k+1)} \|_2^2 \tag{2.103}$$

$$s = A^a r^{(k+1)} \tag{2.104}$$

$$\gamma_s = \| s \|_2^2 \tag{2.105}$$

$$\beta^{(k)} = \gamma_s^{-1} \tag{2.106}$$

$$p^{(k+1)} = p^{(k)} + \beta^{(k)} s^{(k)} \tag{2.107}$$

Terminate when $k = N_g$ or $\sqrt{\frac{\gamma_r}{\gamma_b}} <$ tolerance.

$$\{s\} = \{s_{BI}\} + \{s_{FE}\}. \tag{2.108}$$

where

$$\{s_{BI}\} = \begin{bmatrix} 0 & 0 & 0 & 0 \\ 0 & 0 & 0 & 0 \\ 0 & 0 & 0 & 0 \\ K_1 & 0 & 0 & K_2 \end{bmatrix} \begin{bmatrix} z_1 \\ z_2 \\ z_3 \\ z_4 \end{bmatrix} \tag{2.109}$$

and

$$\{s_{FE}\} = \begin{bmatrix} A_{aa} & A_{aI} & 0 & B_{aa} \\ A_{Ia} & A_{II} & A_{Id} & 0 \\ 0 & 0 & A_{dd} & 0 \\ 0 & 0 & 0 & 0 \end{bmatrix} \begin{bmatrix} z_1 \\ z_2 \\ z_3 \\ z_4 \end{bmatrix} \tag{2.110}$$

For the adjoint operations, we have

$$\{s_{BI}\} = \begin{bmatrix} 0 & 0 & 0 & K_1^a \\ 0 & 0 & 0 & 0 \\ 0 & 0 & 0 & 0 \\ 0 & 0 & 0 & K_2^a \end{bmatrix} \begin{bmatrix} z_1 \\ z_2 \\ z_3 \\ z_4 \end{bmatrix} \tag{2.111}$$

and

$$\{s_{FE}\} = \begin{bmatrix} A^a_{aa} & A^a_{aI} & 0 & 0 \\ A^a_{Ia} & A^a_{II} & A^a_{Id} & 0 \\ 0 & A^a_{dI} & A^a_{dd} & 0 \\ B_{aa} & 0 & 0 & 0 \end{bmatrix} \begin{bmatrix} z_1 \\ z_2 \\ z_3 \\ z_4 \end{bmatrix} \tag{2.112}$$

In each case, the operation is performed such that only the resulting vector $\{s\}$ needs to be stored.

Chapter 3

Scattered Field Computation

In this section the expressions for the scattered field and radar cross-section are developed for both the circular and ogival boundaries. The scattered fields may be computed from the identity

$$\phi^s(\overline{\rho}) = -\oint_{\Gamma_a} \left\{ G(\overline{\rho},\overline{\rho}_a) \left[\frac{\partial}{\partial n_a} \phi(\overline{\rho}_a) \right] - \phi(\overline{\rho}_a) \left[\frac{\partial}{\partial n_a} G(\overline{\rho},\overline{\rho}_a) \right] \right\} d\Gamma_a \tag{3.1}$$

and the echowidth is then found from

$$\sigma = \lim_{\rho \to \infty} 2\pi\rho \frac{|\phi^s|^2}{|\phi^{inc}|^2} \tag{3.2}$$

3.1 Circular Boundary

The scattered field expression (3.1) may be written as

$$\phi^s(\rho,\alpha) = -f_0(\rho,\alpha) + f_1(\rho,\alpha) \tag{3.3}$$

where

$$f_0(\rho,\alpha) = -\frac{j}{4}\rho_a \int_0^{2\pi} \psi(\rho_a,\alpha_a) H_o^{(2)}\left(k_0\sqrt{\rho^2+\rho_a^2-2\rho\rho_a\cos(\alpha-\alpha_a)}\right) d\alpha_a \tag{3.4}$$

and

$$f_1(\rho,\alpha) = \frac{j}{4}\rho_a k_0 \int_0^{2\pi} \phi(\rho_a,\alpha_a) \frac{H_1^{(2)}\left(k_0\sqrt{\rho^2+\rho_a^2-2\rho\rho_a\cos(\alpha-\alpha_a)}\right)}{\sqrt{\rho^2+\rho_a^2-2\rho\rho_a\cos(\alpha-\alpha_a)}} (\rho_a - \rho\cos(\alpha-\alpha_a))\, d\alpha_a \tag{3.5}$$

To evaluate the integrals in (3.4) and (3.5) we invoke the field expansions (2.43) and (2.51). We have

$$f_0(\rho,\alpha) = -\frac{j}{4}\rho_a \sum_{j=1}^{N_a} \hat{\psi}_j \int_{\alpha_j-\frac{\Delta}{2}}^{\alpha_j+\frac{\Delta}{2}} H_o^{(2)}\left(k_0\sqrt{\rho^2+\rho_a^2-2\rho\rho_a\cos(\alpha-\alpha_a)}\right) d\alpha_a \tag{3.6}$$

and

$$f_1(\rho,\alpha) = \frac{j}{4}k_0\rho_a \sum_{j=1}^{N_a} \hat{\phi}_j \int_{\alpha_j-\frac{\Delta}{2}}^{\alpha_j+\frac{\Delta}{2}} \frac{H_1^{(2)}\left(k_0\sqrt{\rho^2+\rho_a^2-2\rho\rho_a\cos(\alpha-\alpha_a)}\right)}{\sqrt{\rho^2+\rho_a^2-2\rho\rho_a\cos(\alpha-\alpha_a)}} (\rho_a - \rho\cos(\alpha-\alpha_a))\, d\alpha_a \tag{3.7}$$

where the remaining integrals over the subsections must be evaluated numerically for arbitrary observation. However, for far-field computations ($\rho \to \infty$), the Hankel functions may be approximated as

$$H_n^{(2)}(k\rho) \sim \sqrt{\frac{2j}{\pi k\rho}} j^n e^{-jk\rho} \tag{3.8}$$

and since

$$\sqrt{\rho^2+\rho_a^2-2\rho\rho_a\cos(\alpha-\alpha_a)} \simeq \begin{cases} \rho & \text{for amplitude} \\ \rho-\rho_a\cos(\alpha-\alpha_a) & \text{for phase terms} \end{cases} \tag{3.9}$$

(3.6) and (3.7) become

$$f_0(\rho,\alpha) = -j\frac{\rho_a\Delta}{4}\sqrt{\frac{2j}{\pi k_0\rho}}e^{-jk_0\rho}\sum_{j=1}^{N_a}\hat{\psi}_j e^{jk_0\rho_a\cos(\alpha-\alpha_j)} \tag{3.10}$$

and

$$f_1(\rho,\alpha) = \frac{\rho_a k_0\Delta}{4}\sqrt{\frac{2j}{\pi k_0\rho}}e^{-jk_0\rho}\sum_{j=1}^{N_a}\hat{\phi}_j\cos(\alpha-\alpha_j)e^{jk_0\rho_a\cos(\alpha-\alpha_j)} \tag{3.11}$$

Substutiting (3.10) and (3.11) into (3.3) we obtain

$$\phi^s_{ff}(\rho,\alpha) = \frac{\rho_a\Delta}{4}\sqrt{\frac{2j}{\pi k_0\rho}}e^{-jk_0\rho}\left[j\sum_{j=1}^{N_a}\hat{\psi}_j e^{jk_0\rho_a\cos(\alpha-\alpha_j)} + k_0\sum_{j=1}^{N_a}\hat{\phi}_j\cos(\alpha-\alpha_j)e^{jk_0\rho_a\cos(\alpha-\alpha_j)}\right] \tag{3.12}$$

and from (3.2) the echowidth is given by yields the echowidth

$$\frac{\sigma}{\lambda} = \sigma_\lambda = \frac{(\rho_a\Delta)^2}{8\pi}\left|j\sum_{j=1}^{N_a}\hat{\psi}_j e^{jk_0\rho_a\cos(\alpha-\alpha_j)} + k_0\sum_{j=1}^{N_a}\hat{\phi}_j\cos(\alpha-\alpha_j)e^{jk_0\rho_a\cos(\alpha-\alpha_j)}\right|^2 \tag{3.13}$$

3.2 Ogival Boundary

Following the same discretization scheme used in Section 2.2.3, (3.1) may be written as

$$\phi^s(\rho,\alpha) = -\Big\{ \sum_{j=1}^{N_{a_1}} \hat{\psi} f_{11}(\rho,\alpha,\alpha_j) + \sum_{j=N_{a_1}+1}^{N_a} \hat{\psi} f_{12}(\rho,\alpha,\alpha_j) - \sum_{j=1}^{N_{a_1}} \hat{\phi} f_{21}(\rho,\alpha,\alpha_j) - \sum_{j=N_{a_1}+1}^{N_a} \hat{\phi} f_{22}(\rho,\alpha,\alpha_j) \Big\} \tag{3.14}$$

where

$$f_{1p}(\rho,\alpha,\alpha_j) = \int_{\alpha_j}^{\alpha_j+\Delta_p} G_o(\rho,\rho_{a_p},\alpha,\alpha_{a_p})\rho_{a_p} d\alpha_{a_p} \tag{3.15}$$

$$f_{2p}(\rho,\alpha,\alpha_j) = \int_{\alpha_j}^{\alpha_j+\Delta_p} \frac{\partial}{\partial \rho_{a_p}} G_o(\rho,\rho_{a_p},\alpha,\alpha_{a_p})\rho_{a_p} d\alpha_{a_p} \tag{3.16}$$

(3.17)

in which

$$G_o(\rho,\rho_{a_p},\alpha,\alpha_{a_p}) = -\frac{j}{4} H_o^{(2)}\left(k_o\sqrt{\rho^2+\rho_{a_p}^2-2\rho\rho_{a_p}\cos(\alpha-\alpha_{a_p})+y_{c_p}^2-2y_{c_p}(\rho\sin\alpha-\rho_{a_p}\sin\alpha_{a_p})}\right) \tag{3.18}$$

and

$$\frac{\partial}{\partial \rho_{a_p}} G_o(\rho,\rho_{a_p},\alpha,\alpha_{a_p}) = \frac{jk_o}{4} \frac{H_1^{(2)}\left(k_o\sqrt{\rho^2+\rho_{a_p}^2-2\rho\rho_{a_p}\cos(\alpha-\alpha_{a_p})+y_{c_p}^2-2y_{c_p}(\rho\sin\alpha-\rho_{a_p}\sin\alpha_{a_p})}\right)}{\sqrt{\rho^2+\rho_{a_p}^2-2\rho\rho_{a_p}\cos(\alpha-\alpha_{a_p})+y_{c_p}^2-2y_{c_p}(\rho\sin\alpha-\rho_{a_p}\sin\alpha_{a_p})}} \left[\rho_{a_p}-\rho\cos(\alpha-\alpha_{a_p})+y_{c_p}\sin\alpha_{a_p}\right] \tag{3.19}$$

and y_{c_p} are the corresponding y-coordinates of the arc Γ_{a_p}. Using the large argument approximation for the Hankel functions

$$\lim_{\rho\to\infty} H_n^{(2)}(k\rho) \sim \sqrt{\frac{2j}{\pi k\rho}} j^n e^{-jk\rho} \tag{3.20}$$

and the approximation

$$\sqrt{\rho + \rho_{a_p}^2 - 2\rho\rho_{a_p}\cos(\alpha-\alpha_{a_p}) + y_{c_p}^2 + 2y_{c_p}(\rho\sin\alpha - \rho_{a_p}\sin\alpha_{a_p})}$$
$$= \begin{cases} \rho & \text{for amplitude terms} \\ \rho - \rho_{a_p}\cos(\alpha-\alpha_{a_p}) + y_{c_p}\sin\alpha & \text{for phase terms} \end{cases} \tag{3.21}$$

for $\rho \to \infty$, the Hankel function simplifies to

$$H_o^{(2)}(\sqrt{\cdot y_{c_p}\cdot})) \sim \sqrt{\frac{2j}{\pi k_o\rho}} e^{-jk_o\rho} e^{-jk_o\left[-\rho_{a_p}\cos(\alpha-\alpha_{a_p})-y_{c_p}\sin\alpha\right]} \tag{3.22}$$

Similarly,

$$\frac{H_1^{(2)}(\sqrt{\cdot y_{c_p}\cdot})}{\sqrt{\cdot y_{c_p}\cdot}}[\cdot y_{c_p}\cdot] \sim -j\sqrt{\frac{2j}{\pi k_o\rho}} e^{-jk_o\rho} e^{-jk_o\left[-\rho_{a_p}\cos(\alpha-\alpha_{a_p})-y_{c_p}\sin\alpha\right]}\cos(\alpha-\alpha_{a_p}) \tag{3.23}$$

Substutiting these into (3.15) and (3.16) and performing midpoint integration yields

$$f_{1p}(\rho,\alpha,\alpha_j) = -j\frac{\Delta_p\rho_{a_p}}{4}\sqrt{\frac{2j}{\pi k_o\rho}} e^{-jk_o\rho} e^{-jk_o\left[-\rho_{a_p}\cos(\alpha-\alpha_j-\frac{\Delta_p}{2})-y_{c_p}\sin\alpha\right]} \tag{3.24}$$

$$f_{2p}(\rho,\alpha,\alpha_j) = k_o\frac{\Delta_p\rho_{a_p}}{4}\sqrt{\frac{2j}{\pi k_o\rho}} e^{-jk_o\rho} e^{-jk_o\left[-\rho_{a_p}\cos(\alpha-\alpha_j-\frac{\Delta_p}{2})-y_{c_p}\sin\alpha\right]}$$
$$\cos(\alpha_j + \frac{\Delta_p}{2} - \alpha_{a_p}) \tag{3.25}$$

Thus, from (3.14)

$$\phi_{ff}^s(\rho,\alpha) = -\frac{1}{4}\sqrt{\frac{2j}{\pi k_o\rho}} e^{-jk_o\rho}\Big\{ -j\Delta_1\rho_{a_1}\sum_{j=1}^{N_{a_1}} \hat{\psi} e^{-jk_o\left[-\rho_{a_1}\cos(\alpha-\alpha_j-\frac{\Delta_1}{2})-y_{c_1}\sin\alpha\right]}$$
$$-j\Delta_2\rho_{a_2}\sum_{j=N_{a_1}+1}^{N_a} \hat{\psi} e^{-jk_o\left[-\rho_{a_2}\cos(\alpha-\alpha_j-\frac{\Delta_2}{2})-y_{c_2}\sin\alpha\right]}$$

$$-k_o\Delta_1\rho_{a_1}\sum_{j=1}^{N_{a_1}}\hat{\phi}e^{-jk_o\left[-\rho_{a_1}\cos(\alpha-\alpha_j-\frac{\Delta_1}{2})-y_{c_1}\sin\alpha\right]}\cos(\alpha_j+\frac{\Delta_1}{2}-\alpha_{a_1})$$

$$-k_o\Delta_2\rho_{a_2}\sum_{j=N_{a_1}+1}^{N_a}\hat{\phi}e^{-jk_o\left[-\rho_{a_2}\cos(\alpha-\alpha_j-\frac{\Delta_2}{2})-y_{c_2}\sin\alpha\right]}\cos(\alpha_j+\frac{\Delta_2}{2}-\alpha_{a_2})\Big\} \quad (3.26)$$

and by substituting this into (3.2) yields the echowidth

$$\frac{\sigma}{\lambda}=\sigma_\lambda=\frac{1}{8\pi}\Big|j\Delta_1\rho_{a_1}\sum_{j=1}^{N_{a_1}}\hat{\psi}e^{-jk_o\left[-\rho_{a_1}\cos(\alpha-\alpha_j-\frac{\Delta_1}{2})-y_{c_1}\sin\alpha\right]}$$

$$+j\Delta_2\rho_{a_2}\sum_{j=N_{a_1}+1}^{N_a}\hat{\psi}e^{-jk_o\left[-\rho_{a_2}\cos(\alpha-\alpha_j-\frac{\Delta_2}{2})-y_{c_2}\sin\alpha\right]}$$

$$+k_o\Delta_1\rho_{a_1}\sum_{j=1}^{N_{a_1}}\hat{\phi}e^{-jk_o\left[-\rho_{a_1}\cos(\alpha-\alpha_j-\frac{\Delta_1}{2})-y_{c_1}\sin\alpha\right]}\cos(\alpha_j+\frac{\Delta_1}{2}-\alpha_{a_1})$$

$$+k_o\Delta_2\rho_{a_2}\sum_{j=N_{a_1}+1}^{N_a}\hat{\phi}e^{-jk_o\left[-\rho_{a_2}\cos(\alpha-\alpha_j-\frac{\Delta_2}{2})-y_{c_2}\sin\alpha\right]}\cos(\alpha_j+\frac{\Delta_2}{2}-\alpha_{a_2})\Big|^2 \quad (3.27)$$

Chapter 4

Results

The scattering patterns of several circular and ogival cylinders for both E- and H-polarization are shown in the figures to follow. Figs. 4.1-4.3 contain circular geometries both coated and uncoated, while Figs. 4.4-4.6 contain coated and uncoated ogival structures. The echowidth is computed for each structure and compared to the results of the series solution for the circular bodies and moment method [5, 4] for the ogival structures. As seen in all cases, the generated patterns via the hybrid BE/FE-CGFFT formulation are in excellent agreement with the corresponding data based on the Mei Series and Moment Method Solutions.

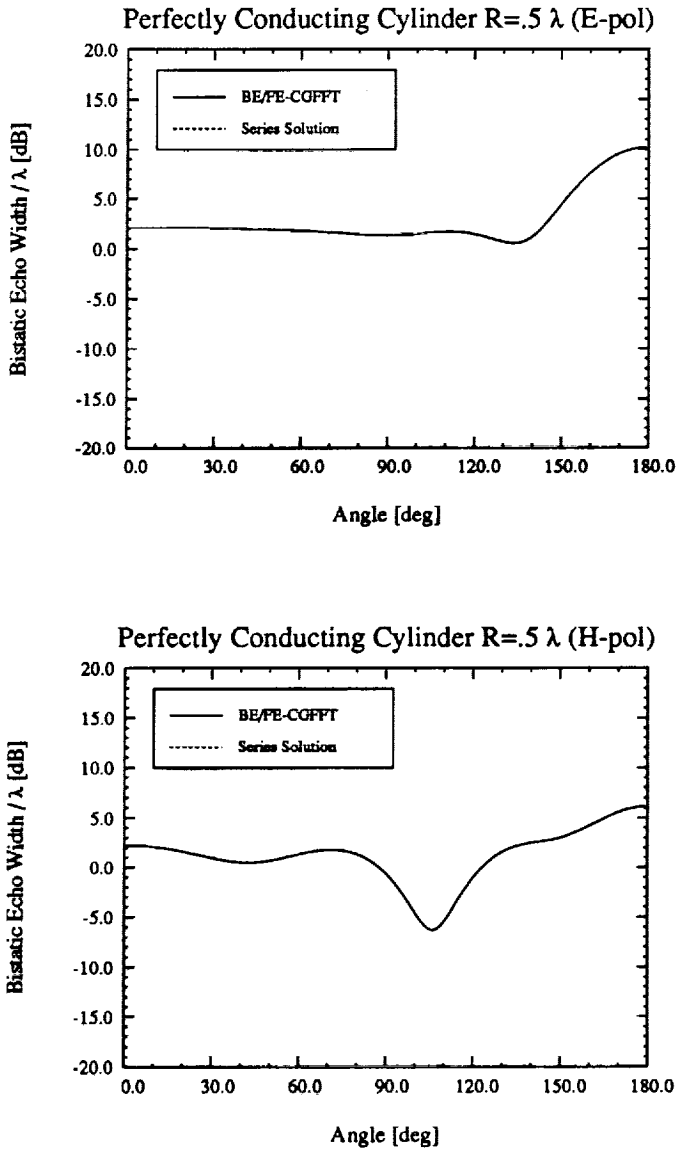

Figure 4.1: E_z and H_z bistatic echowidth from a perfectly conducting circular cylinder of radius 0.5λ.

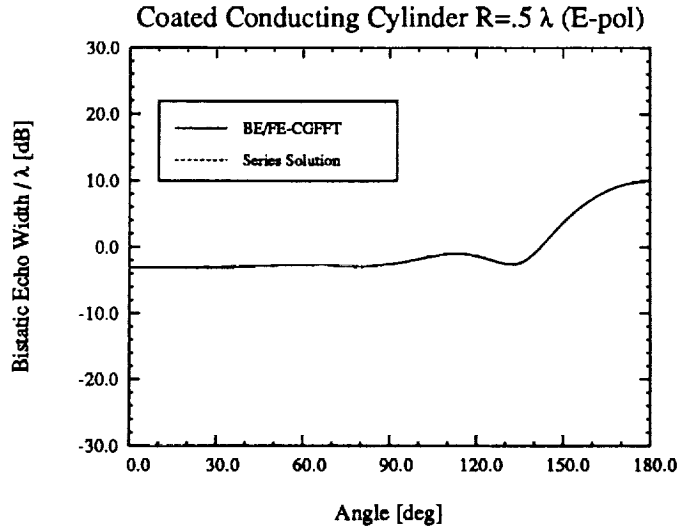

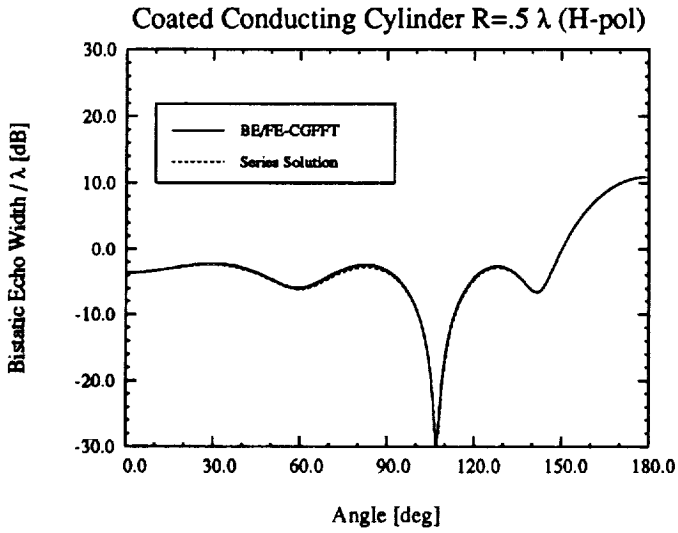

Figure 4.2: E_z and H_z bistatic echowidth from a perfectly conducting circular cylinder with a conductor radius of .5λ and a coating thickness of .05λ containing material properties $\epsilon_r = 5 - j5$, $\mu_r = 1.5 - j0.5$.

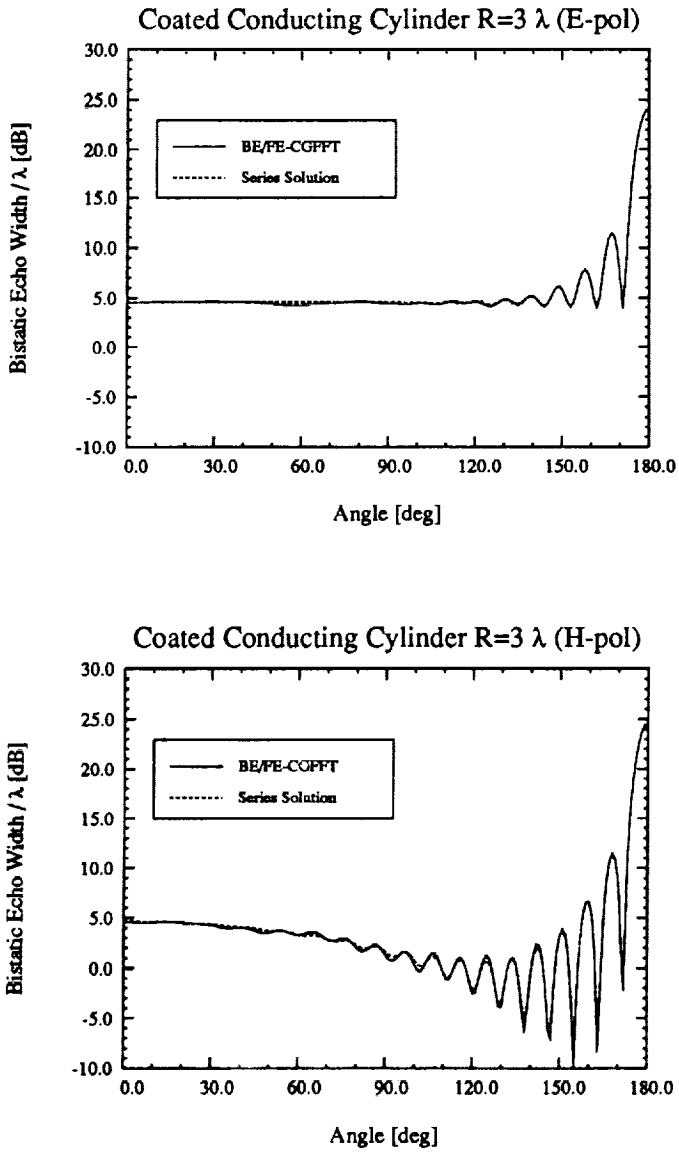

Figure 4.3: E_z and H_z bistatic echowidth from a coated circular cylinder with a conductor radius of 3λ and coating thickness of 0.05λ with material properties $\epsilon_r = 5 - j5$, $\mu_r = 1.5 - j0.5$.

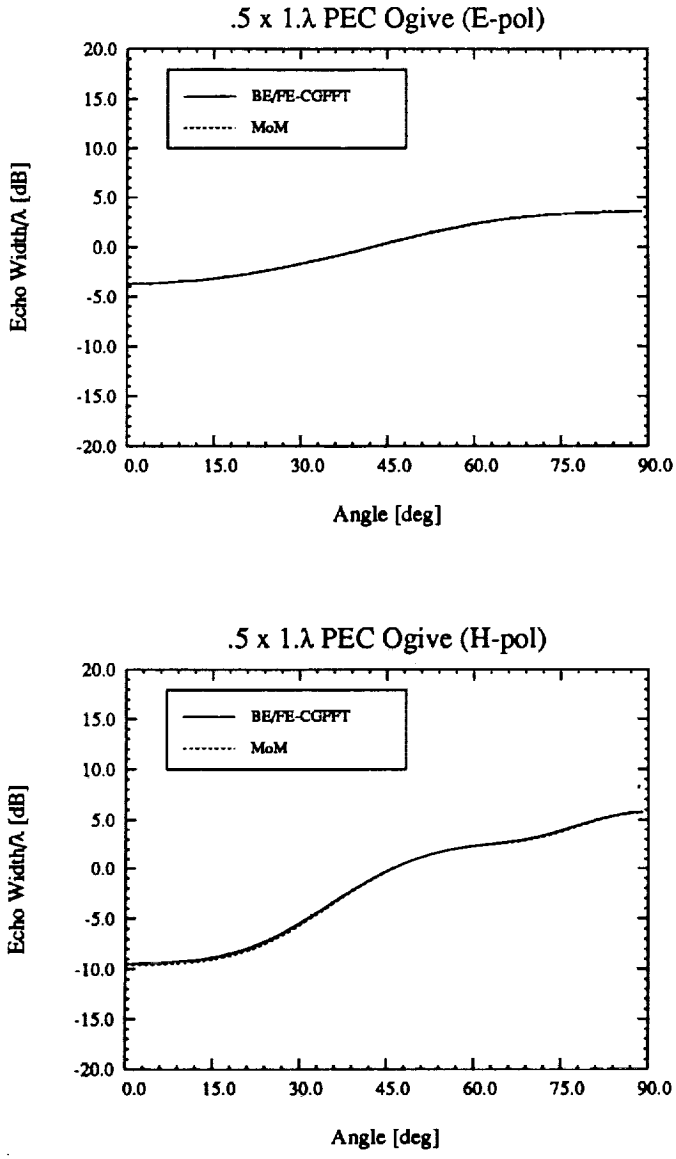

Figure 4.4: E_z and H_z backscatter echowidth from a 0.5 x 1λ perfectly conducting ogive.

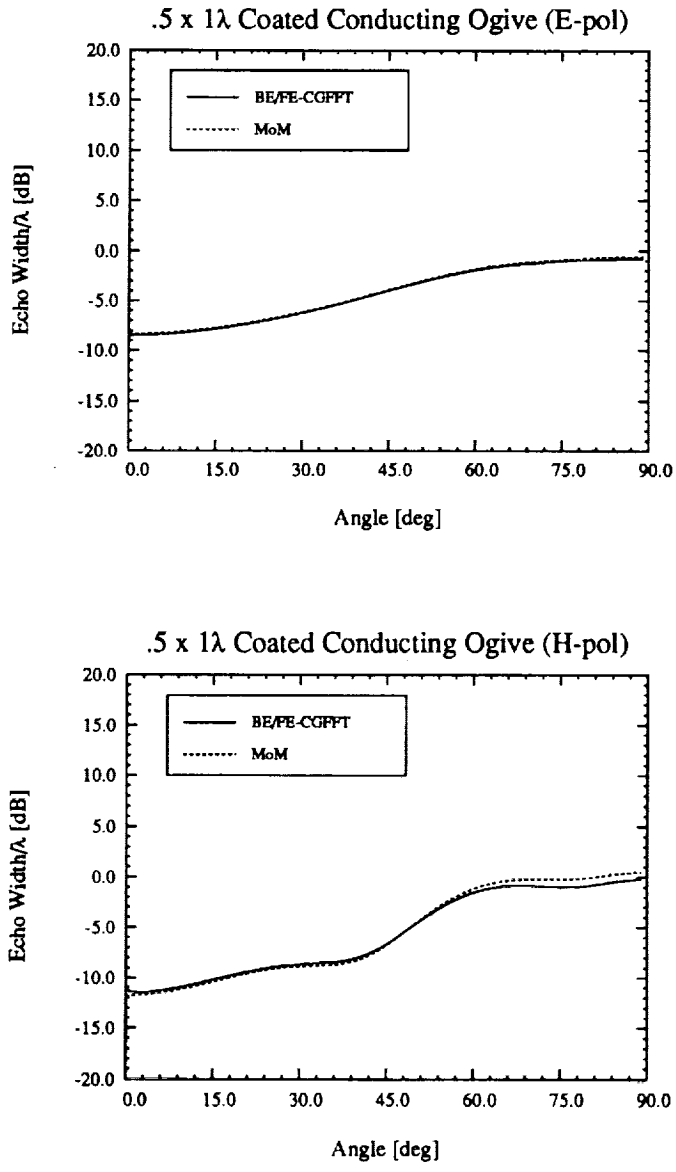

Figure 4.5: E_z and H_z backscatter echowidth from a .5 x 1λ perfectly conducting ogive with a 0.05λ thick material coating containing the properties $\epsilon_r = 3 - j5, \mu_r = 1.5 - j0.5$.

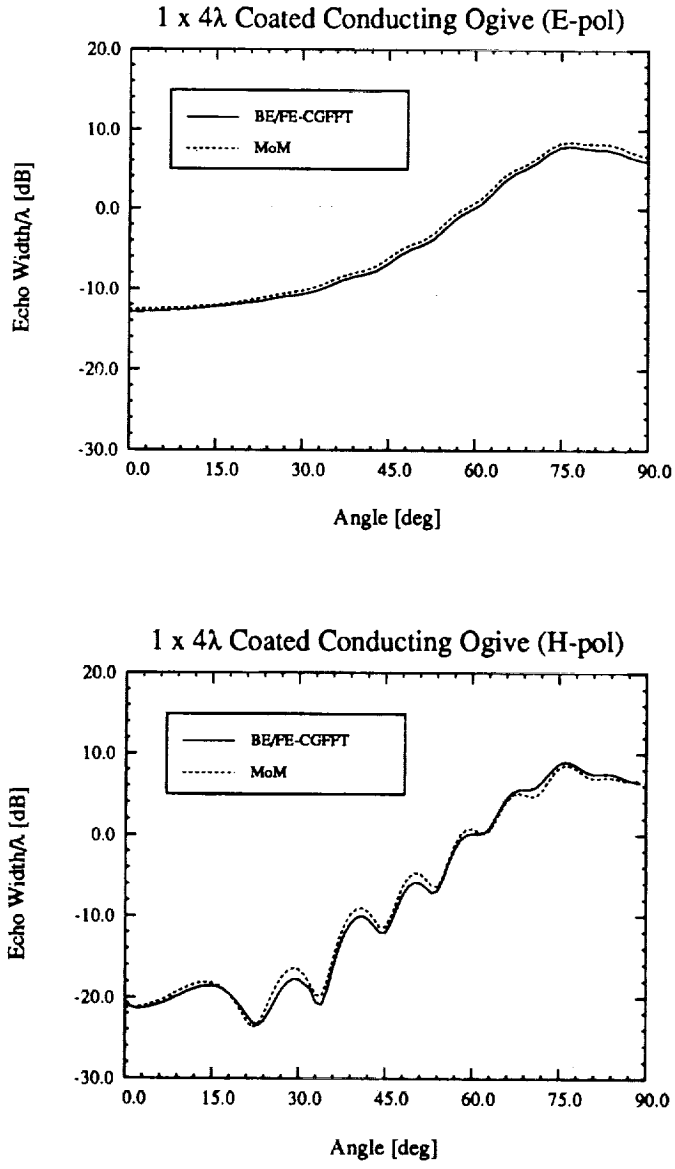

Figure 4.6: E_z and H_z backscatter echowidth from a $1 \times 4\lambda$ perfectly conducting ogive with a $.05\lambda$ thick material coating containing the properties $\epsilon_r = 3 - j5, \mu_r = 1.5 - j0.5$.

Chapter 5

Conclusions and Future Work

The scattering from targets surrounded by ogival and circular boundaries has been presented. The finite element method produces the usual sparse sub-matrix, while a discrete version of the boundary integral results in a dense sub-matrix. The mathematical boundary enclosing the scattering structure may be judiciously chosen such that the boundary integrals are convolutional. As a result, they become amenable to evaluation via the FFT and leads to an $O(N)$ storage requirement. Among the circular and ogival boundaries considered, the circular boundary satisfies the above requirements. The ogival boundary results in convolutions only when the source and observation points are along the same arc, while the non-convolutional cross-terms must be stored efficiently to guarantee the required storage requirement. When considering circular and ogival structures, the associated circular and ogival boundaries are usually conformal to the structure, thus providing an additional reduction in the number of unknowns.

To validate the method and associated computer code, scattering patterns of several circular and ogival structures were given and compared with data generated by proven methods.

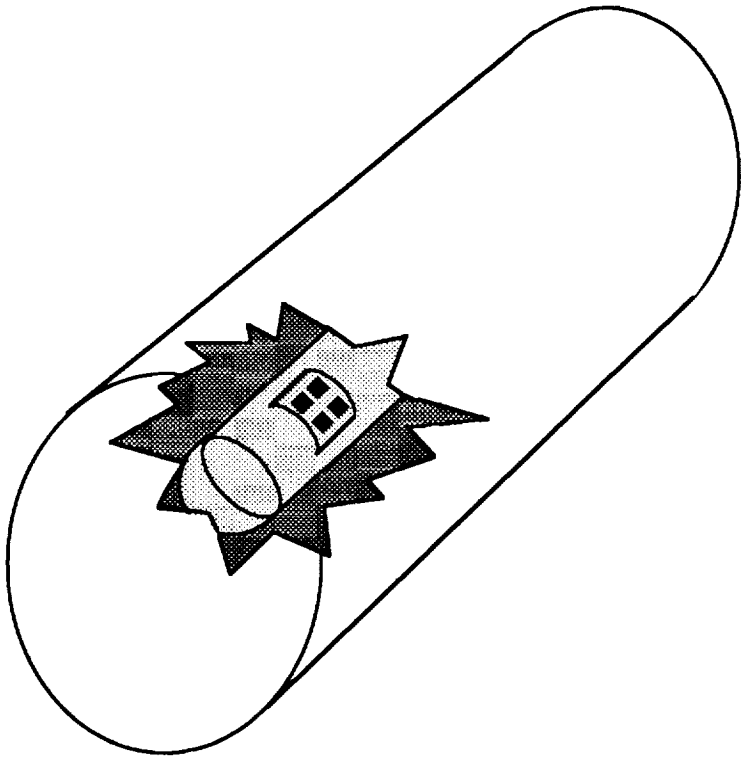

Figure 5.1: Three-dimensional finite-cylinder enclosure.

The fundamental purpose of this work was to explore formulations that lead to $O(N)$ storage requirements when employed for three-dimensional simulations. The presented hybrid technique may prove useful when the surrounding boundary is chosen such that most of the terms of the boundary integral are convolutional. The remaining "cross-terms" however, must be stored efficiently and some sort of interpolation should be used for their evaluation. Based on this study, a suitable three-dimensional enclosure is a truncated circular cylinder as illustrated in Fig. 5.1.

Bibliography

[1] R. Mittra and O. Ramahi, "Absorbing boundary conditions for the direct solution of partial differential equations arising in electromagnetic scattering problems," *PIER 2: Finite Element and Finite Difference Methods in Electromagnetic Scattering*, New York: Elsevier, 1990, pp. 133-174.

[2] K.K. Mei, "Unimoment method of solving antenna and scattering problems," *IEEE Trans. Antennas Prop.*, vol AP-22, pp. 760-766, Nov. 1974.

[3] B.H. McDonald and A. Wexler, "Finite-element solution of unbounded field problems," *IEEE Trans. Microwave Theory Tech.*, vol. MTT-20, pp. 841-847, Dec. 1972.

[4] J.M. Jin and V.V. Liepa, "Simple moment method program for computing scattering from complex cylindrical obstacles," *IEE Proceedings*, Vol. 136, part H, No. 4, pp. 321-329, Aug. 1989.

[5] M.A. Ricoy and J.L. Volakis, "Integral equations with reduced unknowns for the simulation of two-dimensional composite structures," *IEEE Trans. Antennas Propagat.*, Vol. AP-37, pp. 362-372, 1989.

[6] J.D. Collins, J. Jin and J.L. Volakis, "A combined finite element-boundary integral formulation for solution via CGFFT of two-dimensional scattering problems", submitted to AP-S.

[7] K. Barkeshli and J.L. Volakis, stuff concerning the circular strip

[8] Brebbia, C.A. and Dominguez, J., *Boundary Elements: An Introductory Course*, New York: McGraw-Hill, 1989.

[9] O.C. Zienkewicz and K. Morgan, *Finite Elements and Approximation*, New York: Wiley, 1983.

[10] Harrington, R.F., *Time-Harmonic Electromagnetic Fields*, New York: McGraw-Hill, 1961, p. 203.